# Improvement of tunneling magnetoresistance and spin-valley polarization in magnetic silicene superlattices induced by structural disorder

O. Oubram●
*Facultad de Ciencias Químicas e Ingeniería, Universidad Autónoma del Estado de Morelos, Avenida Universidad 1001, Colonia Chamilpa, 62209 Cuernavaca, Morelos, Mexico*

J. G. Rojas-Briseño ●, S. Molina-Valdovinos ●, and I. Rodríguez-Vargas ●*
*Unidad Académica de Ciencia y Tecnología de la Luz y la Materia, Universidad Autónoma de Zacatecas, Carretera Zacatecas-Guadalajara Km. 6, Ejido La Escondida, 98160 Zacatecas, Zacatecas, Mexico*

It is well known that the unavoidable variation of the heights and widths of the barriers (structural disorder) in semiconductor superlattices and superlattices based on two-dimensional materials degrades important physical properties such as the electronic transport and the thermoelectric response. Here, we show that the structural disorder contrary to what is expected improves the magnetoresistive and spin-valleytronic properties of magnetic silicene superlattices. We reach this conclusion by studying the impact of the random variations of the width and strength of the magnetic barriers on the tunneling magnetoresistance and spin-valley polarization. The theoretical treatment is based on a Dirac-like Hamiltonian, the transfer matrix method, and the Landauer-Büttiker formalism to describe silicene electrons, to obtain the transmittance, and to obtain the conductance, respectively. Our results indicate that structural disorder effects improve the magnetoresistance response and the spin-valley polarization by eliminating the conductance oscillations caused by the periodic magnetic modulation as well as by differentiating the response of the conductance for the parallel and antiparallel magnetization configuration. These results could be useful in designing versatile devices with magnetoresistive and spin-valleytronic capabilities. Particularly, magnetic silicene superlattices with moderate structural disorder are more convenient than perfect or nearly perfect ones.

## I. INTRODUCTION

Superlattices based on two-dimensional (2D) materials are quite attractive from both the fundamental and technological standpoint. In the case of graphene, a periodic potential gives rise to peculiar characteristics such as extra Dirac points in the band structure and highly anisotropic group velocities of the charge carriers [1–4]. In addition, graphene superlattices have been instrumental to corroborate/uncover exotic phenomena such as the Hofstadter butterfly [4–6], Brown-Zak fermions [7], unconventional superconductivity [8,9], and correlated electron-hole states [10]. There are also important breakthroughs in the fabrication of gated graphene superlattices [11,12]. These superlattices are quite relevant for applications due to the possible modulation of the physical properties through applied gate voltage. In the case of silicene, the implementation of periodic potentials to modulate its physical properties is not the exception. Silicene [13–15], a low-buckled 2D material with a large spin-orbit coupling [16], a local band gap [16,17] modulable with an external electric field [18,19], and differentiable spin-valley degrees of freedom, is ideal for spin-valleytronic applications. In fact, silicene superlattices have been used to optimize the spin-valley

polarization [20–32] and/or magnetoresistance [32–34]. The periodic potential gives rise to oscillating transport properties with significant differences in the spin-valley components and/or the magnetization configurations. For instance, Zhang *et al.* [20] studied the spin-valley dependent transport in silicene superlattices under the combined effect of an exchange field, a perpendicular electric field, and a gate voltage, finding that the spin-valley polarization is a sensitive oscillatory function of the gate voltage, switching from 100% to −100% by a slight change of the applied voltage. Similarly, Lu *et al.* [22] studied the spin-valley dependent energy band and transport properties of silicene under a periodic potential. They found that the Dirac points, minibands, band gap, group velocity, and conductance are highly dependent on the spin-valley indices. Moreover, the spin-valley dependent band structure can be used to modulate the electronic transport, resulting in remarkable spin-valley polarizations switchable by the structural parameters and greatly enhanced by the disorder of the periodic potential. Here, it is important to mention that in most works the optimization of the spin-valley polarization is achieved through a periodic gate voltage in combination with an exchange field, electric field, strain, Fermi velocity barriers, or polarized light. It is also worth mentioning that the magnetoresistive response is not addressed in these reports. A significant magnetoresistance can be obtained in silicene by modulating it in magnetic periodic fashion [32–34]. More
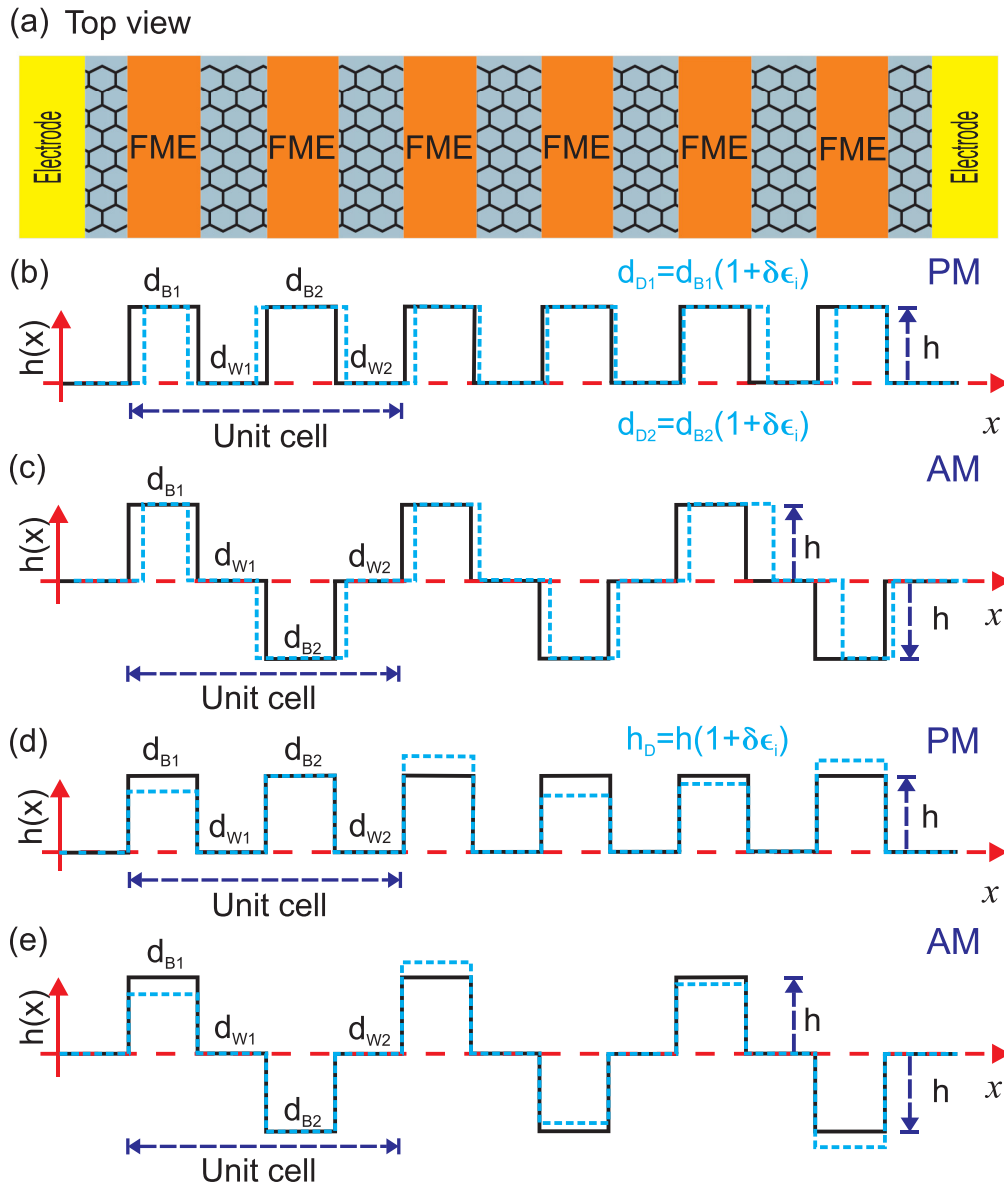
*isaac@uaz.edu.mx

FIG. 1. (a) Schematic representation of disordered magnetic silicene superlattices. Magnetic superlattice profile for the parallel (PM) and antiparallel (AM) magnetization configuration with structural disorder associated to the (b, c) width and (d, e) strength of the magnetic barriers. The dashed cyan lines correspond to disordered superlattices, while the solid black lines correspond to ordered ones.

importantly, versatile silicene structures with magnetoresistive and spin-valley polarization capabilities could be possible by modulating the exchange field periodically [32]. By inducing structural asymmetry in the so-called magnetic silicene superlattices (MSSLs) an enhancement of more than an order of magnitude is achieved for the tunneling magnetoresistance (TMR) with respect to single magnetic junctions as well as two well-defined spin-valley polarization states switchable by reversing the magnetization direction.

The performance of superlattices can be degraded by the unavoidable variation of its structural parameters. In fact, it is well documented that the structural disorder associated to the width of barriers and wells and the strength of the barriers can greatly modify the transport properties of graphene and silicene superlattices [22,35–39]. For instance, the conductance

of disordered graphene superlattices of various thicknesses which fluctuate randomly around a mean value was studied [35]. It was found that the charge carriers that approach to the barriers at nearly normal incidence transmit throughout the superlattice structure regardless of the intensity of the disorder. Furthermore, for some specific conditions the conductance tends to a finite value when the superlattice size becomes very large, in contrast to semiconductor superlattices. The effect of strain fluctuations on the transport properties of strain-induced graphene superlattices was studied [37]. It was found that the number of peaks in the transmission disappears with the strain white noise disorder. Moreover, negative strains are more relevant on the conductance than positive ones, and the conductance decreases as the strength of strain fluctuations increases. Regarding gated silicene superlattices, there are also studies addressing the impact of structural disorder on
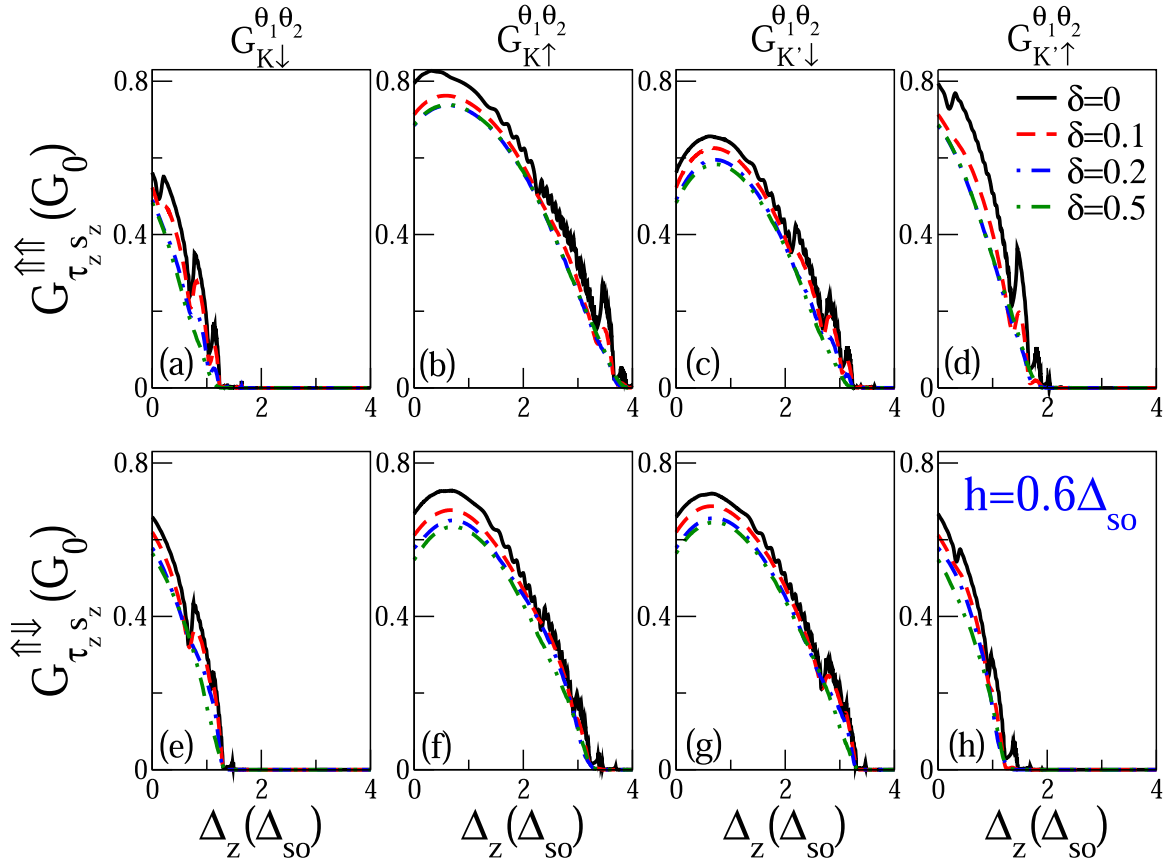
FIG. 2. Spin-valley conductance components $G_{\tau_z s_z}^{\theta_1 \theta_2}$ of D-MSSLs as a function of $\Delta_z$ at different intensities of the disorder ($\delta$) associated to the widths of the magnetic barriers $d_{D1} = d_{B1}(1 + \delta\epsilon_i)$ and $d_{D2} = d_{B2}(1 + \delta\epsilon_i)$. The first and second column correspond to the spin-down and -up conductance components of the $K$ valley, while the third and fourth column correspond to the spin-down and -up ones of the $K'$ valley. The first and second row correspond to the parallel (PM) and antiparallel (AM) magnetic configuration of the spin-valley conductance components. The energy of the charge carriers, the strength of the magnetic barriers, the width of barrier wells, and the number of superlattice periods are $E = 3.0\Delta_{SO}$, $h = 0.6\Delta_{SO}$, $d_{B1} = 2.0l_{SO}$, $d_{W1} = 1.0l_{SO}$, $d_{B2} = 3.0l_{SO}$, $d_{W2} = 2.0l_{SO}$, and $N = 10$, respectively.

the transport and thermoelectric properties [38,39]. In the case of the transport properties [38], it is reported that the conductance oscillates as a function of the height of the barriers and decreases as the size of the system increases. In addition, the conductance diminishes as the intensity of the disorder associated to the width of the barriers increases. In the case of the thermoelectric properties [39], it was found that the structural disorder associated to the strength of the barriers is more relevant than the corresponding one to the width of the barriers and the on-site potential. In particular, the fluctuations of the strength of the electrostatic barriers induce a strong suppression on the conductance, Seebeck coefficient, and power factor. So, to preserve the thermoelectric performance of gated silicene superlattices is fundamental to have a precise control of the strength of the barriers. Here, it is worth mentioning that, according to our knowledge, there are no studies addressing the impact of structural disorder on the transport properties of MSSLs. Taking into account the relevance of MSSLs for tunneling magnetoresistance and spin-valley polarization [32], we consider that a thorough assessment of the impact of structural disorder on the transport properties of MSSLs is needed.

In this paper, we show that structural disorder, contrary to what is typically expected, improves the tunneling magnetoresistance and spin-valley polarization of MSSLs. We reach this conclusion by studying the effects of structural disorder on spin-valley components of the conductance for the parallel and antiparallel magnetization configuration of MSSLs. Our theoretical treatment based on a relativistic description of the charge carriers, the transfer matrix method, and the Landauer-Büttiker formalism tells us that the tunneling magnetoresistance and spin-valley polarization improvement is related to the suppression of the oscillations in the conductance as well as the differentiated response of the conductance for the parallel and antiparallel magnetization configuration caused by the structural disorder of the width and strength of the magnetic barriers. So, in designing versatile magnetoresistive and spin-valleytronic superlattice devices it is better to allow moderate structural disorder instead of trying to eliminate it.

The rest of the paper is organized as follows: In Sec. II the details of disordered MSSLs (D-MSSLs) are presented along with the theoretical model used to obtain the transmission and transport properties. In Sec. III we analyze the main results of the tunneling magnetoresistance and the spin-valley polarization under the effects of structural disorder. Finally, we summarize our paper by highlighting the most relevant points in Sec. IV.
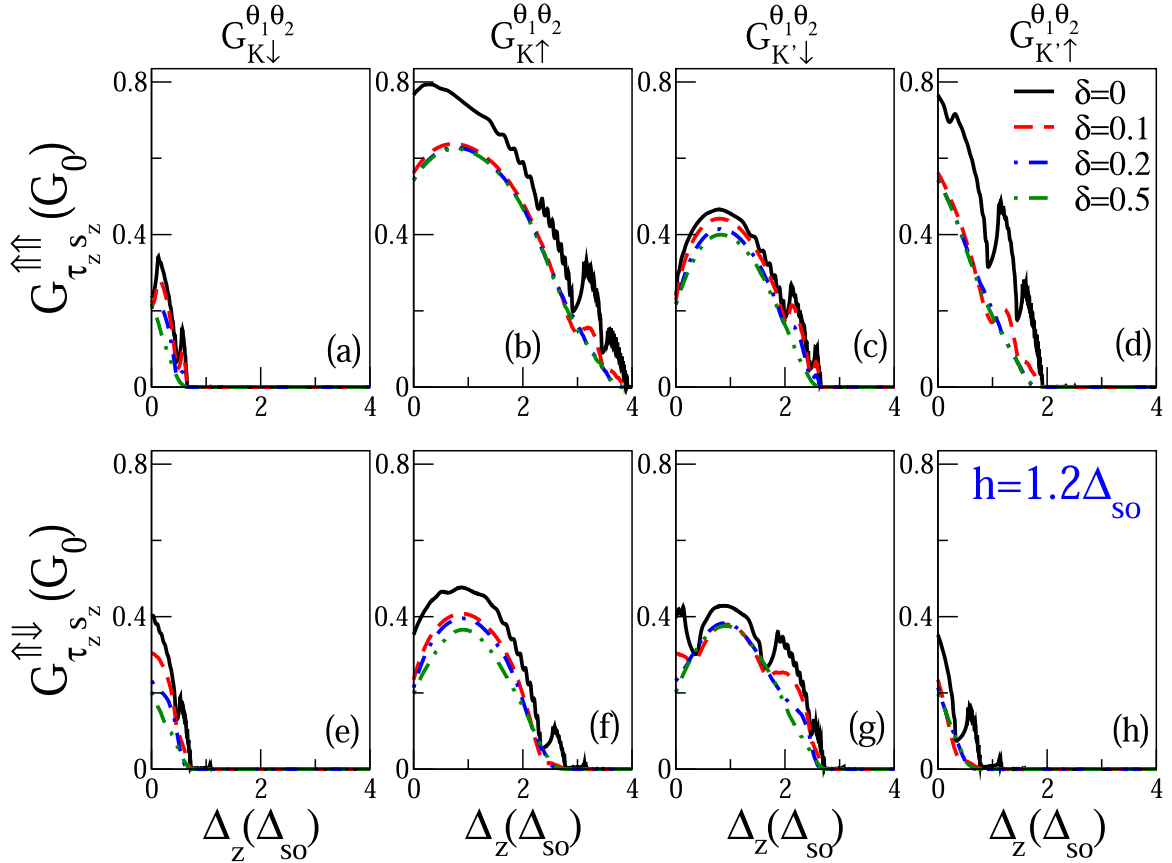
FIG. 3. The same as Fig. 2, but here the strength of the magnetic barriers is $h = 1.2\Delta_{\text{SO}}$.

## II. THEORETICAL MODEL

The unavoidable variation (disorder) of the magnetic barriers generated by the ferromagnetic electrodes (FMEs) in a superlattice structure like the one depicted in Fig. 1 creates what we called D-MSSLs. The superlattice structure consists of a silicene sheet placed on a noninteracting substrate, atop FMEs arranged in periodic fashion and left-right metallic electrodes. The magnetic superlattice profiles shown in Figs. 1(b)–1(e) are generated through magnetic proximity effect between the silicene sheet and the FMEs. As the width and the strength of the magnetic barriers are not perfect there is a natural structural disorder. The random variation of the width of the magnetic barriers at a specific disorder intensity gives rise to a disordered magnetic profile for the parallel and antiparallel magnetization configuration as shown in Figs. 1(b) and 1(c), respectively. The same happens for the random variation of the strength of the barriers as represented in Figs. 1(d) and 1(e). MSSLs are composed of unit cells with two barriers and two wells, with the second barrier being the soft region allowing us to change the magnetization configuration from parallel to antiparallel by simply reversing its magnetization direction. The structural disorder associated to the width of the barriers is accounted for by considering variations of the width of the unit-cell barriers according to $d_{D1} = d_{B1}(1 + \delta\epsilon_i)$ and $d_{D2} = d_{B2}(1 + \delta\epsilon_i)$, $d_{B1}$ and $d_{B2}$ being the nominal widths of the barriers, $\delta$ the disorder intensity, and $\epsilon_i$ a random number that lies between 1 and $-1$. Likewise, the disorder associated to the strength of the barriers is considered through $h_D = h(1 + \delta\epsilon_i)$, $h$ being the nominal strength of the magnetic barriers, and $\delta$ and $\epsilon_i$ with the same meaning as in the case of the disorder related to the width of the barriers. It is important to mention that all barriers are subjected to the same disorder intensity, however its variation is totally random through $\epsilon_i$; in other words, D-MSSLs cannot be obtained by simply replicating a unit cell as in the case of perfect MSSLs [32].

The model to describe the charge carriers and obtain the transport properties of D-MSSLs is essentially the same used in perfect MSSLs [32]. So, we will outline it, highlighting the most relevant points as well as the modifications demanded by structural disorder.

The charge carriers are described by the low-energy effective Hamiltonian [16–18,40,41]

$$\hat{H} = v_F(p_x\sigma_x - \tau_z p_y\sigma_y) - (s_z\tau_z\Delta_{\text{SO}} - \Delta_z(x))\sigma_z - s_z h(x),$$
(1)

where

$$h(x) = \begin{cases} \theta h_D & \text{for barriers} \\ 0 & \text{for wells.} \end{cases}$$
(2)

The other parameters are the Fermi velocity $v_F$, the two-dimensional momentum $\vec{p} = (p_x, p_y)$, the Pauli matrices $\vec{\sigma} = (\sigma_x, \sigma_y, \sigma_z)$, the spin-orbit interaction energy $\Delta_{\text{SO}}$, the on-site potential (local band gap) $\Delta_z(x)$, the valley index $\tau_z$, the spin index $s_z$, and the magnetization configuration parameter $\theta$.
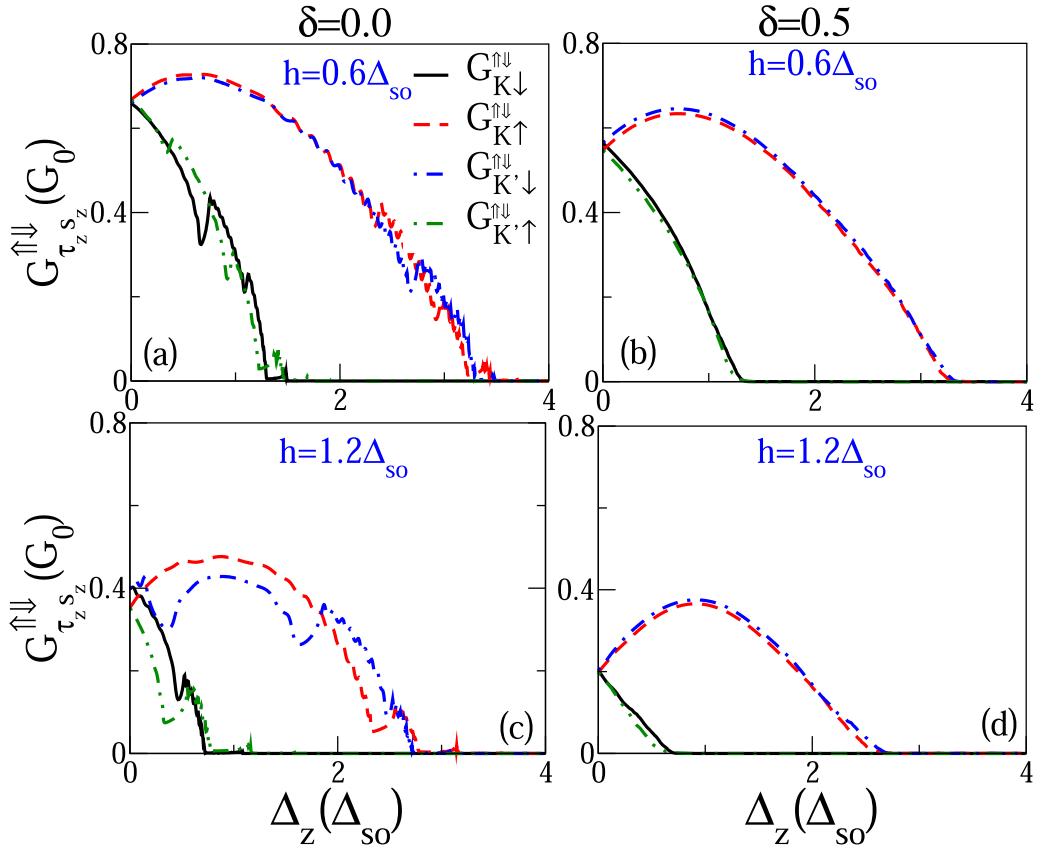
FIG. 4. Alternate crossover between the spin-valley conductance components of the antiparallel magnetization configuration of ordered ($\delta = 0.0$) MSSLs for (a) $h = 0.6\Delta_{SO}$ and (c) $h = 1.2\Delta_{SO}$. Suppression of the alternate crossover by the structural disorder ($\delta = 0.5$) of the width of the barriers for (b) $h = 0.6\Delta_{SO}$ and (d) $h = 1.2\Delta_{SO}$. The other superlattice parameters are the same as in Fig. 2.

The eigenvalue problem in the barrier, well, and semi-infinite regions can be solved straightforwardly due to the constant exchange field in these regions. In particular, the wave function in the barrier regions is given by [32]

$$\psi^b(x, y) = A_+^b \begin{pmatrix} 1 \\ v_+^b \end{pmatrix} e^{iq_x^b x + iq_y^b y} + A_-^b \begin{pmatrix} 1 \\ v_-^b \end{pmatrix} e^{-iq_x^b x + iq_y^b y}, \quad (3)$$

where

$$v_\pm^b = \frac{\hbar v_F (\pm q_x^b - i\tau_z q_y^b)}{E + s_z \theta h_D - (\tau_z s_z \Delta_{SO} - \Delta_z)} \quad (4)$$

and

$$q_x^b = \frac{1}{\hbar v_F} \sqrt{(E + s_z \theta h_D)^2 - (\tau_z s_z \Delta_{SO} - \Delta_z)^2 - (\hbar v_F q_y^b)^2}. \quad (5)$$

Here, it is important to highlight that the structural disorder associated to the strength of the barriers is involved directly in the bispinor coefficients $v_\pm^b$ and wave vector $q_x^b$. In addition, the wave functions and wave vectors of the well (semi-infinite) regions can be readily obtained by setting $h_D = 0$ (and $\Delta_z = 0$).

The calculation of the transmission coefficient is based on the well-known transfer matrix method. By requiring the continuity of the wave function along the superlattice structure

as well as the conservation of the transverse momentum it is possible to obtain a relationship between the coefficients of the wave function in the left semi-infinite region $A_+^L$ and $A_-^L$ and the corresponding ones in the right semi-infinite region $A_+^R$ and $A_-^R$ in terms of the transfer matrix of the disordered superlattice structure $M^{DSL}$, namely,

$$\begin{pmatrix} A_+^L \\ A_-^L \end{pmatrix} = M^{DSL} \begin{pmatrix} A_+^R \\ A_-^R \end{pmatrix}, \quad (6)$$

where

$$M^{DSL} = M_{UC1}^{DSL} M_{UC2}^{DSL} \cdots M_{UCN}^{DSL} \quad (7)$$

and

$$M_{UCj}^{DSL} = M_{b1}^D M_{w1} M_{b2}^D M_{w2}. \quad (8)$$

Here, $M_{UCj}^{DSL}$ is the transfer matrix of the $j$th unit-cell of the disordered superlattice structure, and $M_{b1}^D$ ($M_{b2}^D$) and $M_{w1}$ ($M_{w2}$) are the transfer matrices of the first (second) barrier and well within the unit cell. The transfer matrices of the barrier regions are given by

$$M_{b1}^D = D_0^{-1} \left( D_{b1}^D P_{b1}^D (D_{b1}^D)^{-1} \right) D_0, \quad (9)$$

$$M_{b2}^D = D_0^{-1} \left( D_{b2}^D P_{b2}^D (D_{b2}^D)^{-1} \right) D_0, \quad (10)$$
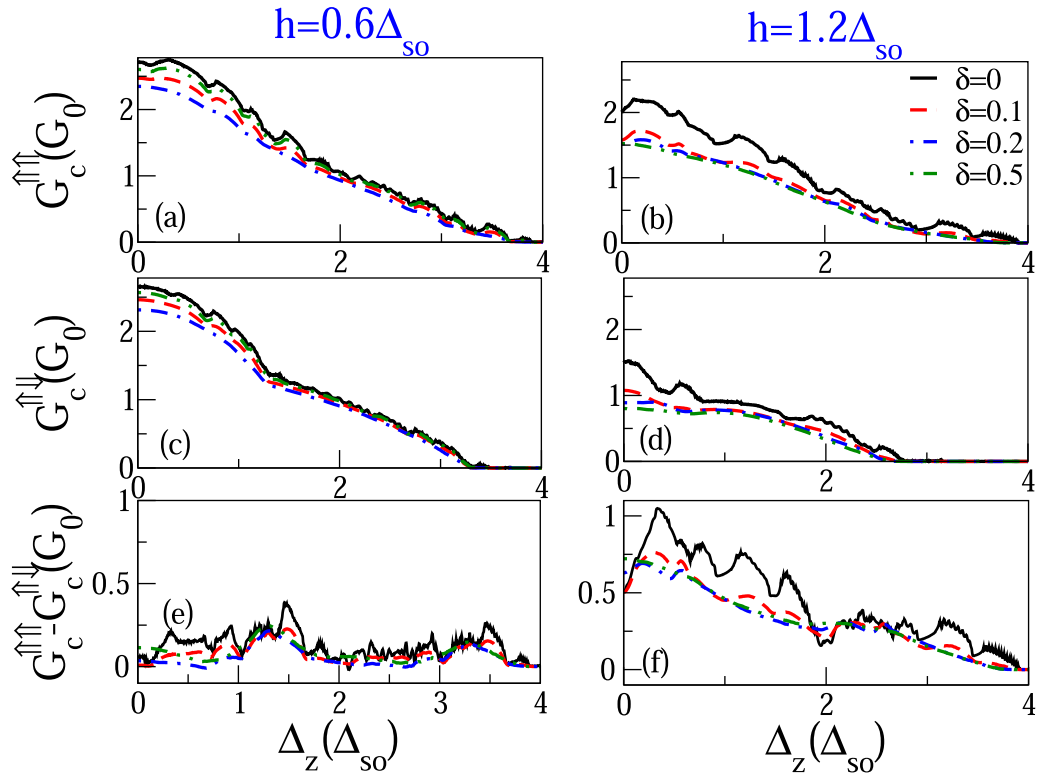
FIG. 5. Total conductance $G_c^{\theta_1\theta_2}$ of D-MSSLs as a function of $\Delta_z$ at different disorder intensities associated to the widths of the barriers. The first, second, and third row correspond to the total conductance of the PM and the AM and the difference between them $G_c^{\Uparrow\Uparrow} - G^{\Uparrow\Downarrow}$, respectively. The exchange field strengths considered are (first column) $h = 0.6\Delta_{\text{SO}}$ and (second column) $h = 1.2\Delta_{\text{SO}}$. The other superlattice parameters are the same as in Fig. 2.
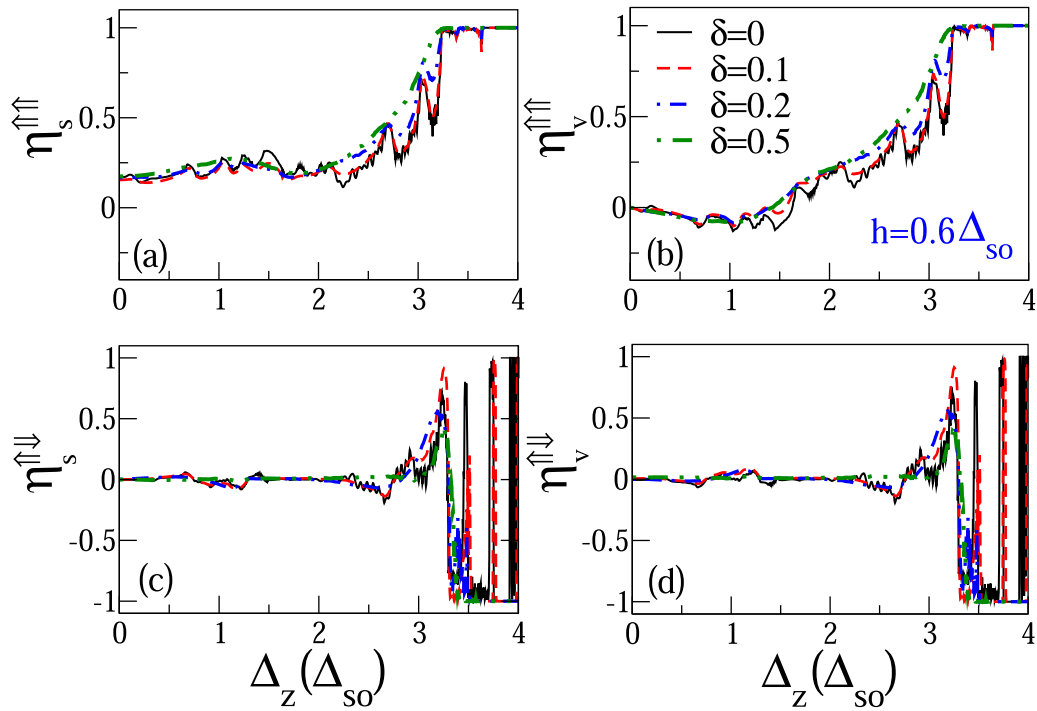


FIG. 6. (First column) Spin and (second column) valley polarization of D-MSSLs as a function of $\Delta_z$ at different intensities of the disorder associated to the widths of the barriers. The first and second row correspond to PM and AM, respectively. The strength of the exchange field is $h = 0.6\Delta_{\text{SO}}$. The other superlattice parameters are the same as in the preceding figures.
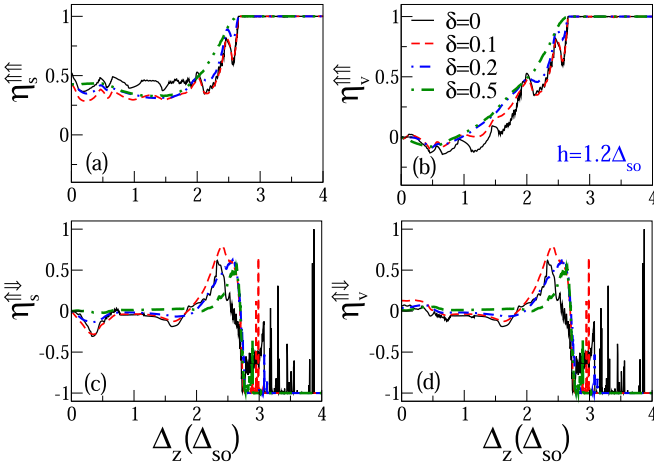
FIG. 7. The same as Fig. 6, but here the strength of the exchange field is $h = 1.2\Delta_{SO}$.

with $D_0$ the dynamic matrix of the semi-infinite regions, and $D_{b1}^D$ ($D_{b2}^D$) and $P_{b1}^D$ ($P_{b2}^D$) the dynamic and propagation matrices of the first (second) barrier. The dynamic matrices are given by

$$D_{b1}^D = \begin{pmatrix} 1 & 1 \\ v_+^{b1} & v_-^{b1} \end{pmatrix}, \quad D_{b2}^D = \begin{pmatrix} 1 & 1 \\ v_+^{b2} & v_-^{b2} \end{pmatrix}, \quad (11)$$

and the propagation matrices are given by

$$P_{b1}^D = \begin{pmatrix} e^{-iq_x^{b1}d_{D1}} & 0 \\ 0 & e^{iq_x^{b1}d_{D1}} \end{pmatrix}, \quad P_{b2}^D = \begin{pmatrix} e^{-iq_x^{b2}d_{D2}} & 0 \\ 0 & e^{iq_x^{b2}d_{D2}} \end{pmatrix}. \quad (12)$$

As we can notice the structural disorder associated to the width of the magnetic barriers is incorporated in the calculations through the propagation matrices $P_{b1}^D$ and $P_{b2}^D$. The details of the dynamic and propagation matrices of the semi-infinite and well regions can be found in [32].
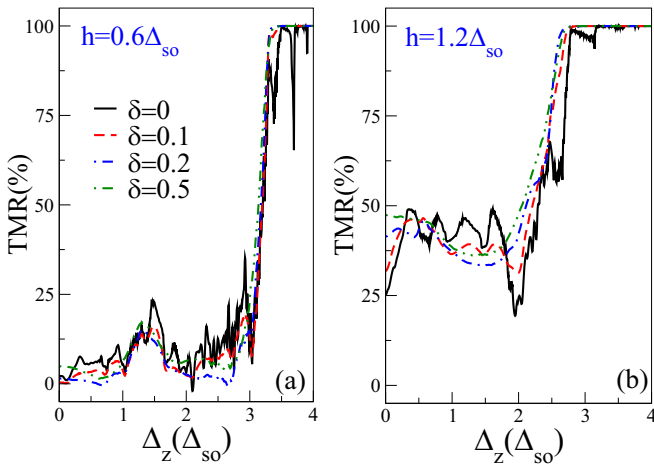


FIG. 8. TMR of D-MSSLs as a function of $\Delta_z$ at different intensities of the disorder associated to the widths of the magnetic barriers. The exchange field strengths considered are (a) $h = 0.6\Delta_{SO}$ and (b) $h = 1.2\Delta_{SO}$. The other superlattice parameters are the same as in the preceding figures.

The transmission coefficient is given by

$$T_{\tau_z s_z}^{\theta_1 \theta_2} = \frac{1}{\left| M_{11}^{DSL} \right|^2}, \quad (13)$$

$M_{11}^{DSL}$ being the (1,1) element of $M^{DSL}$.

The linear-regime conductance at zero temperature can be computed by summing over all transmission channels:

$$G_{\tau_z s_z}^{\theta_1 \theta_2} = G_0 \int_{-\pi/2}^{\pi/2} T_{\tau_z s_z}^{\theta_1 \theta_2} \cos \phi \, d\phi, \quad (14)$$

where $G_0$ and $\phi$ are the fundamental conductance factor and the angle of incidence of the impinging electrons on the superlattice structure, respectively.

The magnetoresistive properties are defined in terms of the total charge conductance $G_c^{\theta_1 \theta_2} = \sum_{\tau_z s_z} G_{\tau_z s_z}^{\theta_1 \theta_2}$. In particular, the TMR is given by [42,43]

$$\text{TMR} = \frac{G_c^{\Uparrow\Uparrow} - G_c^{\Uparrow\Downarrow}}{G_c^{\Uparrow\Uparrow}}, \quad (15)$$

where $G_c^{\Uparrow\Uparrow}$ and $G_c^{\Uparrow\Downarrow}$ are the total charge conductance of the PM and AM configuration, respectively.

Finally, the conductance spin polarization can be calculated by weighing the difference between the spin conductance components in the valleys and the total charge conductance as follows:

$$\eta_s^{\theta_1 \theta_2} = \frac{\sum_{\tau_z} \left( G_{\tau_z \uparrow}^{\theta_1 \theta_2} - G_{\tau_z \downarrow}^{\theta_1 \theta_2} \right)}{G_c^{\theta_1 \theta_2}}. \quad (16)$$

In a similar fashion, the conductance valley polarization is determined by weighing the difference between the valley conductance components for the spins and the total charge conductance:

$$\eta_v^{\theta_1 \theta_2} = \frac{\sum_{s_z} \left( G_{K s_z}^{\theta_1 \theta_2} - G_{K' s_z}^{\theta_1 \theta_2} \right)}{G_c^{\theta_1 \theta_2}}. \quad (17)$$

## III. RESULTS AND DISCUSSION

Now, it is time to analyze the main results of the impact of the structural disorder on the tunneling magnetoresistance and the spin-valley polarization. We will first discuss the results of the structural disorder associated to the width of the barriers, then we will proceed with the main outcomes of the disorder related to the strength of the barriers. In both cases we consider asymmetric MSSLs due to the effective spin-valley polarization presented for the antiparallel magnetization configuration [32]. We will consider ordered superlattices or superlattices without disorder $\delta = 0.0$, superlattices with low disorder $\delta = 0.1$ and 0.2, and superlattices with moderate disorder $\delta = 0.5$. The energy of the charge carriers and the superlattice structural parameters will be the same throughout the paper. Specifically, $E = 3.0\Delta_{SO}$, $d_{B1} = 2.0l_{SO}$, $d_{W1} = 1.0l_{SO}$, $d_{B2} = 3.0l_{SO}$, $d_{W2} = 2.0l_{SO}$, and $N = 10$. It is also important to mention that the spin-valley conductance components and the total conductance, which are the base for the calculation of the spin-valley polarization and the tunneling magnetoresistance, are obtained by averaging over more than 200 disorder superlattice configurations. These
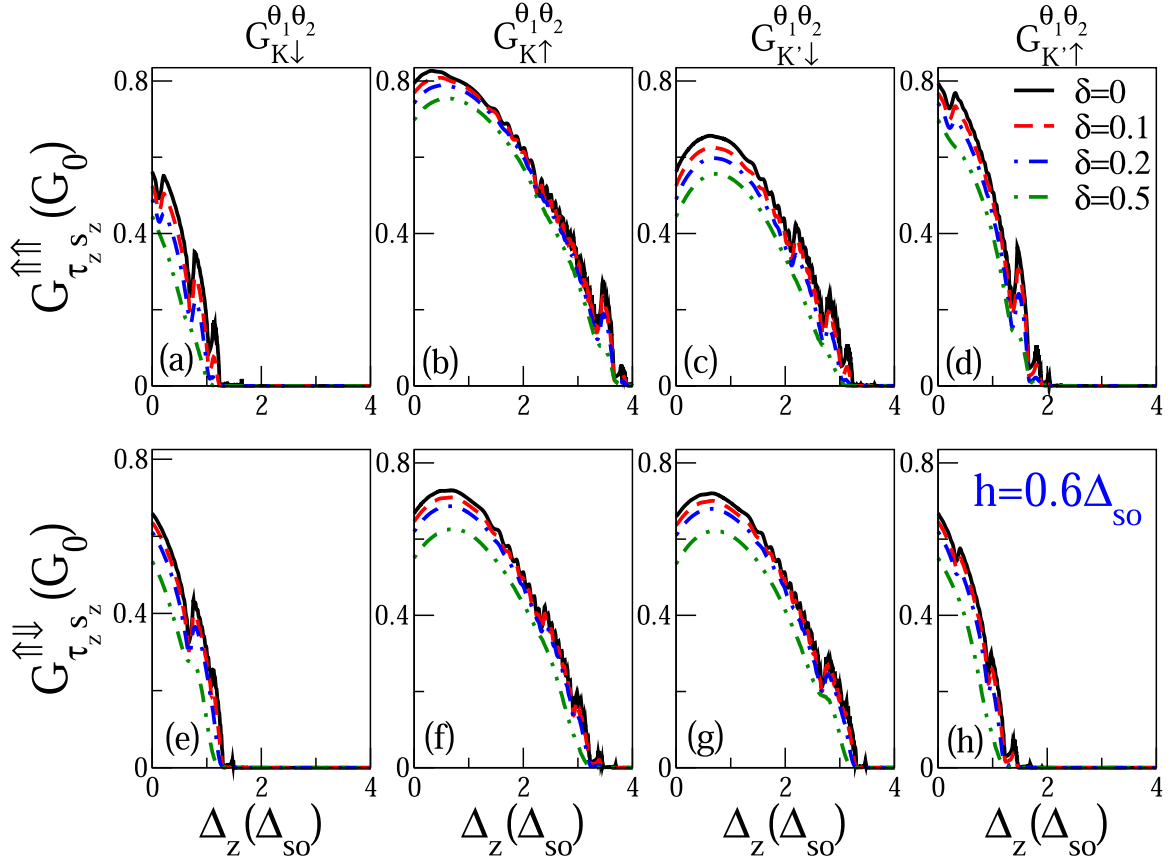
FIG. 9. Spin-valley conductance components $G^{\theta_1\theta_2}$ of D-MSSLs as a function of $\Delta_z$ at different disorder intensities associated to the strength of the magnetic barriers $h_D = h(1 + \delta\epsilon_i)$. The first and second column correspond to the spin-down and -up conductance components of the $K$ valley, while the third and fourth column correspond to the spin-down and -up ones of the $K'$ valley. The first and second row correspond to the PM and AM configuration of the spin-valley conductance components. The superlattice parameters are the same as in Fig. 2.

configurations ensure the convergence of the spin-valley polarization and TMR calculations. To the best of our knowledge this number of configurations is far above the one required for the calculation of the thermoelectric properties in silicene superlattices [39] and the transport properties in semiconductor superlattices [44].

In Fig. 2 we show the effects of the disorder of the width of the barriers on the different spin-valley conductance components of D-MSSLs for (first row) the parallel and (second row) the antiparallel magnetization configuration. The solid-black, dashed-red, dot-dashed-blue, and dot-dashed-green curves correspond to $\delta = 0.0, 0.1, 0.2$ and $0.5$, respectively. In this case the strength of the exchange field is $h = 0.6\Delta_{SO}$. As we can see for ordered superlattices the periodic modulation gives rise to oscillating transport properties [32]. In particular, the spin-valley conductance components present oscillating-descending envelopes as a function of $\Delta_z$ for both parallel and antiparallel magnetization configurations. However, once the structural disorder of the width of the barriers is incorporated two main effects take place in practically all spin-valley conductance components and magnetization configurations: (1) a systematic diminishment of the conductance and (2) an attenuation of the descending envelopes and the oscillations within them. These effects are strengthened as the disorder

intensity rises. It is also important to mention that the reduction of the conductance for the spin-down component in both valleys and both magnetization configurations is gradual as the disorder intensity increases (see the first and third column of Fig. 2). In the case of the spin-up component the conductance in both valleys and both magnetization configurations falls significantly at low disorder intensities and gradually reduces with the disorder intensity (see the second and fourth column of Fig. 2). Similar results are obtained if we increase the strength of the exchange field to $h = 1.2\Delta_{SO}$ (see Fig. 3). However, in this case the reduction of the conductance for the spin-up component in both valleys and both magnetization configurations is intensified, being practically the same for all disorder intensities (see the second and third column of Fig. 3). In the case of the spin-down component the reduction of the conductance is still gradual with the disorder intensity (see the first and third column of Fig. 3). In addition, the alternate crossover between the spin-valley components of the antiparallel magnetization configuration of ordered MSSLs is eliminated by the structural disorder of the width of the barriers as shown in Fig. 4. As we can notice the alternate crossover is presented between $G^{\Uparrow\Downarrow}_{K\uparrow}$ and $G^{\Uparrow\Downarrow}_{K'\downarrow}$ as well as between $G^{\Uparrow\Downarrow}_{K\downarrow}$ and $G^{\Uparrow\Downarrow}_{K'\uparrow}$ (see the results for $\delta = 0.0$, first column of Fig. 4). The difference between the curves involved in the
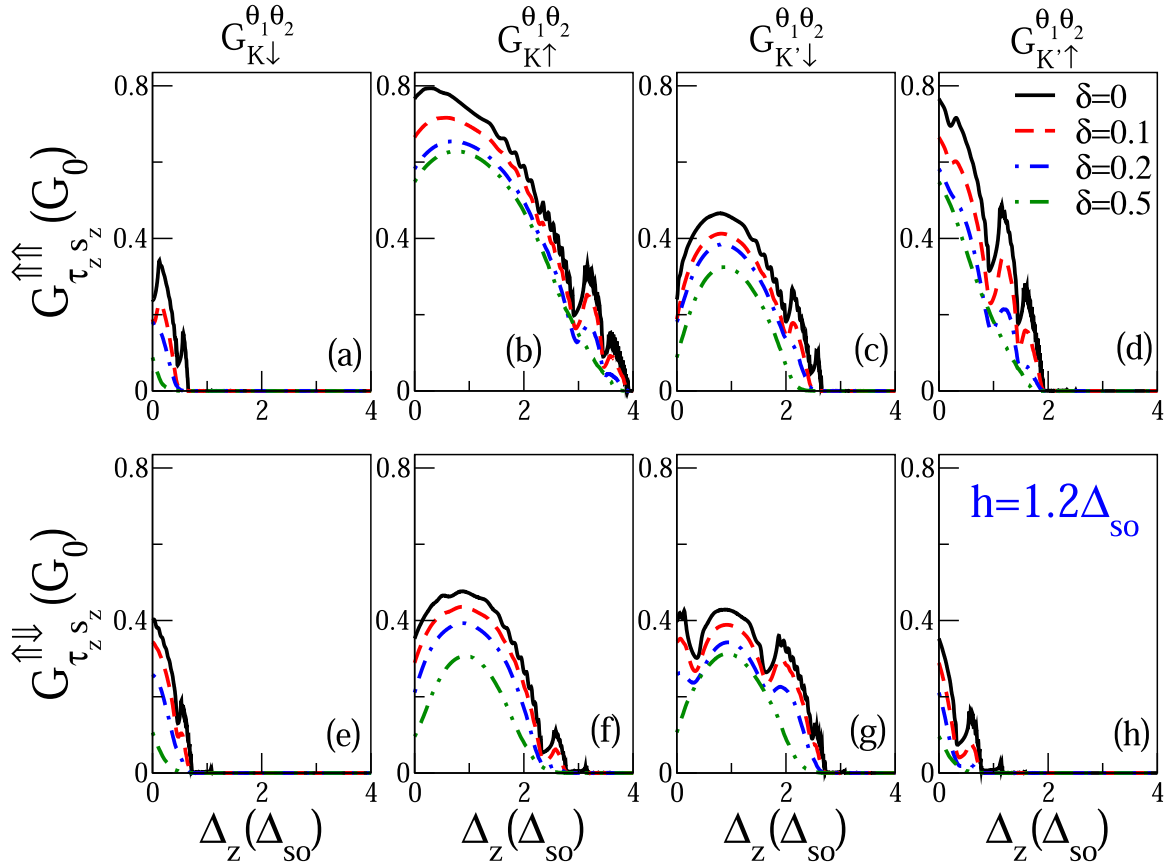
FIG. 10. The same as Fig. 9, but here the strength of the exchange field is $h = 1.2\Delta_{SO}$.

alternate crossover is greater as the strength of the exchange field gets larger [compare the results for $h = 0.6\Delta_{SO}$ and $1.2\Delta_{SO}$ in Figs. 4(a) and 4(c), respectively]. The alternate crossover is to a great extent suppressed by the structural disorder of the width of the barriers for both $h = 0.6\Delta_{SO}$ and $1.2\Delta_{SO}$ [see Figs. 4(b) and 4(d)]. The suppression of this alternate crossover between the spin-valley components will have a great impact on the spin-valley polarization of the antiparallel magnetization configuration. The results of the total conductance for the (first row) parallel and (second row) antiparallel magnetization configuration and its (third column) difference are shown in Fig. 5. The first and second column correspond to $h = 0.6\Delta_{SO}$ and $1.2\Delta_{SO}$, respectively. The effects of the disorder of the width of the barriers are similar as for the spin-valley conductance components. In the case of $h = 0.6\Delta_{SO}$ the total conductance for both parallel and antiparallel magnetization configuration as well as its difference reduces gradually as the disorder intensity increases [see Figs. 5(a), 5(c) and 5(e), respectively]. The oscillations of the total conductances and its difference typical of ordered superlattices are also suppressed with the disorder of the width of the barriers. In the case of $h = 1.2\Delta_{SO}$ the total conductance for both parallel and antiparallel magnetization configuration and its difference reduces considerably at low disorder intensity, followed by a slight reduction at higher disorder intensities as shown in Figs. 5(b), 5(d) and 5(f). So, disorder effects have a greater impact on the total conductances and its difference as the

strength of the exchange field increases. All these characteristics are the result of the disruption of the resonant tunneling conditions caused by the random variation of the width of the barriers as well as the averaging of the spin-valley conductance components over more than 200 disorder superlattice configurations. Moreover, these characteristics will have a significant impact on the spin-valley polarization and the TMR.

In Fig. 6 the effects of the disorder of the width of the barriers on the (first column) spin and (second column) valley polarization are shown. The first and second panel row correspond to the parallel and antiparallel magnetization configuration, respectively. In this case the exchange field strength is $h = 0.6\Delta_{SO}$. As we can notice the spin-valley polarization of ordered superlattices reflects the oscillating characteristics of the transport properties [32]. More importantly, there are energy windows of nearly perfect spin-valley polarization for $\Delta_z > 3.3\Delta_{SO}$ [32]. Specifically, the parallel magnetization configuration shows a positive 100% spin-valley polarization, while the antiparallel magnetization configuration presents alternate regions of negative and positive 100% spin-valley polarization. The main effect of the barriers width disorder is a systematic reduction of spin-valley polarization oscillations as the disorder intensity increases. For low disorder there is a small reduction of the oscillations, while for moderate disorder the oscillations practically disappeared. This effect is more dramatic in the antiparallel magnetization configuration [see Figs. 6(c) and 6(d)]. In
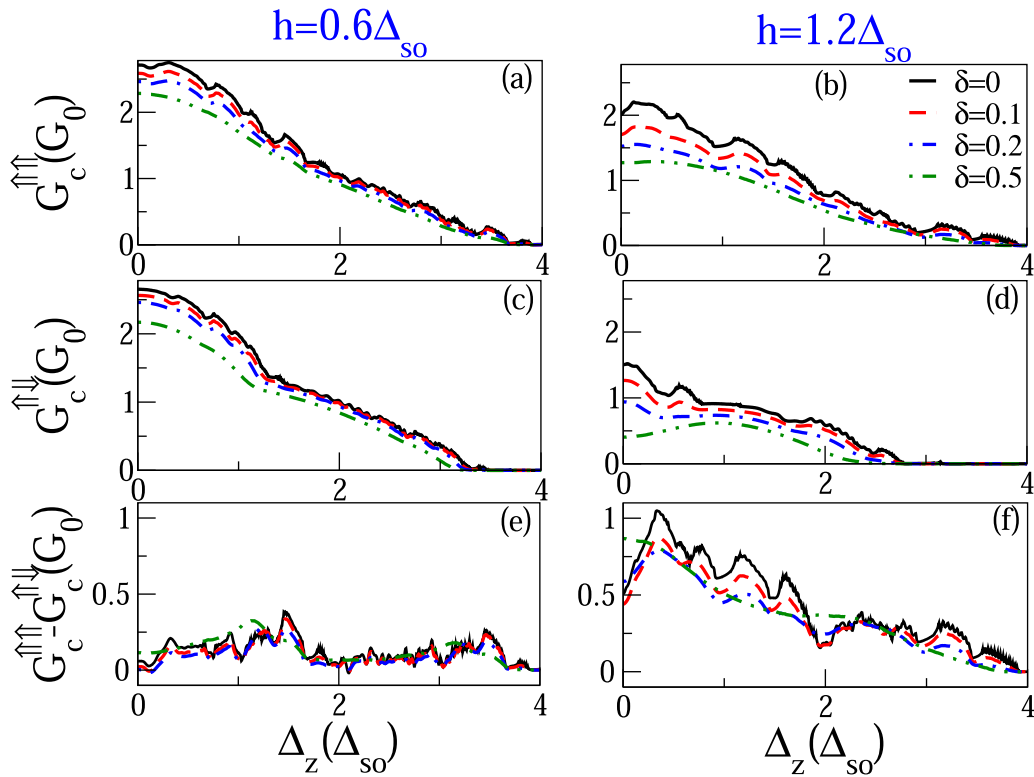
FIG. 11. Total conductance $G_c^{\theta_1\theta_2}$ of D-MSSLs as a function of $\Delta_z$ at different intensities of the disorder associated to the strength of the magnetic barriers. The first, second, and third row correspond to the total conductance of the PM and the AM and the difference between them $G_c^{\Uparrow\Uparrow} - G^{\Uparrow\Downarrow}$, respectively. The exchange field strengths considered are (first column) $h = 0.6\Delta_{SO}$ and (second column) $h = 1.2\Delta_{SO}$. The other superlattice parameters are the same as in Fig. 9.

this case the alternate regions of negative and positive 100% spin-valley polarization are transformed in a region of exclusively negative 100% spin-valley polarization. This is quite relevant because with moderate disorder we can have two well-defined (100%) spin-valley polarization states reachable by simply changing the magnetization configuration. Similar results are obtained for $h = 1.2\Delta_{SO}$ (see Fig. 7). The increase in $h$ brings an enlargement of the region of perfect spin-valley polarization. For the parallel magnetization configuration this region starts at $\Delta_z = 2.5\Delta_{SO}$, while for the antiparallel configuration the region starts around $\Delta_z = 3.0\Delta_{SO}$. We can also see an enhancement of the spin polarization for the parallel magnetization configuration in the interval $(0.0\Delta_{SO}, 2.0\Delta_{SO})$, going from 25% for $h = 0.6\Delta_{SO}$ to 50% for $h = 1.2\Delta_{SO}$ [compare Figs. 6(a) and 7(a)]. The magnetoresistance properties are also affected by the barrier width disorder (see Fig. 8). The periodic magnetic modulation results in an oscillating TMR with regions of 100% magnetoresistance. For $h = 0.6\Delta_{SO}$ [Fig. 8(a)] we can see an oscillating TMR that rises as $\Delta_z$ increases, reaching values of more than 90% after $\Delta_z = 3.3\Delta_{SO}$. The main effect of the barrier width disorder is the systematic reduction of the magnetoresistance oscillations as the disorder intensity increases, flattening the high TMR region and transforming it in a region of 100% TMR. Similar results are obtained for $h = 1.2\Delta_{SO}$ [see Fig. 8(b)]. However, the increase of $h$ results in an overall enhancement of the TMR as well as an enlargement of the high TMR region.

In particular, the region of 100% TMR now starts at about $\Delta_z = 3.0\Delta_{SO}$.

Now, it is time to analyze the impact of the structural disorder associated to the strength of the magnetic barriers. In Figs. 9–11 we show the spin-valley conductance components and the total conductance as a function of $\Delta_z$ for different disorder intensities of the strength of the barriers. The distribution of rows and columns is the same as in the case of the figures of the structural disorder of the width of the barriers. As we can notice the effects of the disorder of the strength of the barriers are similar to the ones caused by the disorder of the width of the barriers; that is, the conductance oscillations are attenuated as the disorder intensity increases, disappearing practically at moderate disorder. The disorder of the strength of the barriers also suppresses the alternate crossover between the spin-valley conductance components of the antiparallel configuration as shown in Fig. 12. In the case of $h = 0.6\Delta_{SO}$ the alternate regions between $G_{K\uparrow}^{\Uparrow\Downarrow}$ and $G_{K'\downarrow}^{\Uparrow\Downarrow}$ as well as between $G_{K\downarrow}^{\Uparrow\Downarrow}$ and $G_{K'\uparrow}^{\Uparrow\Downarrow}$ have been reduced, however not eliminated completely [see Fig. 12(b)]. By increasing the strength of the exchange field up to $h = 1.2\Delta_{SO}$ the alternate crossover is practically eliminated as shown in Fig. 12(d). These characteristics will be reflected in the spin-valley polarization of the antiparallel magnetization configuration. Despite the similarities, the origin of the disorder effects of the strength of the barriers is different from the corresponding one to the disorder effects of the width of the
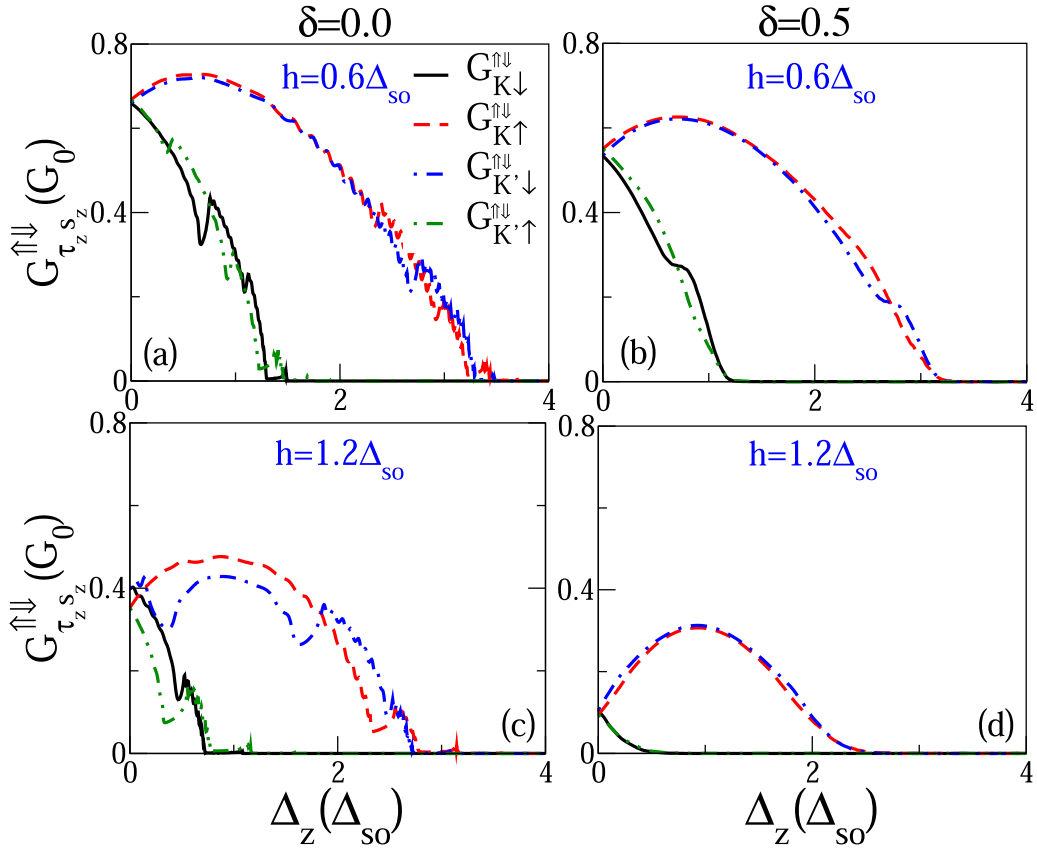
FIG. 12. Alternate crossover between the spin-valley conductance components of the antiparallel magnetization configuration of ordered ($\delta = 0.0$) MSSLs for (a) $h = 0.6\Delta_{SO}$ and (c) $h = 1.2\Delta_{SO}$. Suppression of the alternate crossover by the structural disorder ($\delta = 0.5$) of the strength of the barriers for (b) $h = 0.6\Delta_{SO}$ and (d) $h = 1.2\Delta_{SO}$. The other superlattice parameters are the same as in Fig. 9.

barriers. In the present case, the disorder modifies the character of the charge carriers as well as the bispinor coefficients by changing the propagation wave vector $q_x^b = q_x^b(h_D)$. These modifications greatly affect the propagation characteristics, transforming propagating states to evanescent states and vice versa depending on the specific spin-valley component. As in the case of the disorder of the width of the barriers the reduction of the conductance oscillations with the disorder intensity is beneficial for the spin-valley polarization and the tunneling magnetoresistance (see Figs. 13–15). For $h = 0.6\Delta_{SO}$ the alternate regions of negative and positive 100% spin-valley polarization in the antiparallel magnetization configuration still persist at moderate disorder as shown in Figs. 13(c) and 13(d). By increasing the strength of the exchange field ($h = 1.2\Delta_{SO}$) these regions transform in a region of negative 100% spin-valley polarization as shown in Figs. 14(c) and 14(d), opening the door for two well-defined spin-valley polarization states reachable by switching the magnetization configuration. In the case of the tunneling magnetoresistance the disorder of the strength of the barriers flattens the regions of high TMR, giving rise to a region of 100% TMR that can be enlarged by increasing the strength of the exchange field [see Figs. 15(a) and 15(b)].

Finally, it is important to remark that in the present paper the Saxena definition of the TMR was used [43]. This alter-

native definition allows us to analyze diverging regions of the traditional TMR definition. These regions correspond to 100% TMR for the alternative definition. As the structural disorder eliminates the TMR oscillations, flattening the high TMR regions, it would be very difficult to analyze the structural disorder effects with the traditional TMR definition. The typical TMR peaks assessed with the traditional TMR definition are also accessible with the Saxena TMR definition. For instance, we can analyze readily the impact of the structural disorder on the TMR peak located around $\Delta_z = 2.5\Delta_{SO}$ for $h = 1.2\Delta_{SO}$. In particular, the TMR value of this peak enhances with the intensity of the structural disorder, approaching to 100% TMR at moderate disorder [see Fig. 15(b)].

## IV. CONCLUSIONS

In summary, we have studied the effects of structural disorder on the transport properties of MSSLs. In particular, we have assessed the impact of the disorder associated to the width and strength of the magnetic barriers on the magnetoresistance and spin-valley polarization. The theoretical treatment was based on a quantum relativistic description of the charge carriers through a low-energy effective Hamiltonian. The transfer matrix method and the Landauer-Büttiker formalism were used to obtain the transmission and trans-
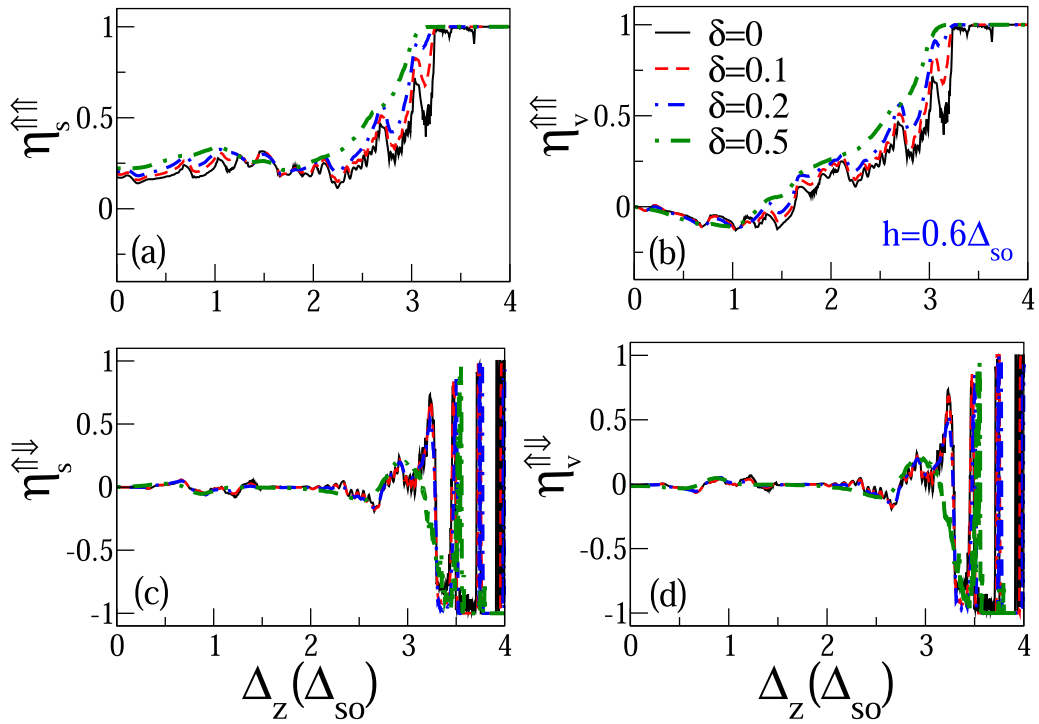
FIG. 13. (First column) Spin and (second column) valley polarization of D-MSSLs as a function of $\Delta_z$ at different intensities of the disorder associated to the strength of the magnetic barriers. The first and second row correspond to PM and AM, respectively. The strength of the exchange field is $h = 0.6\Delta_{\mathrm{SO}}$. The other superlattice parameters are the same as in the preceding figures.
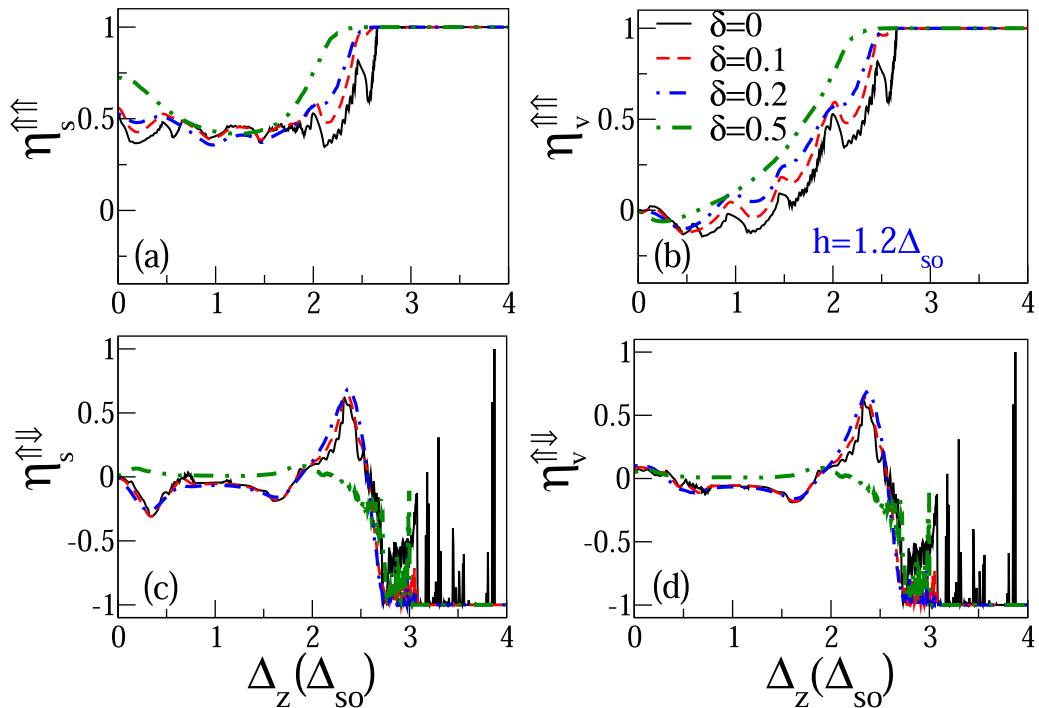


FIG. 14. The same as Fig. 13, but here the strength of the exchange field is $h = 1.2\Delta_{\mathrm{SO}}$.
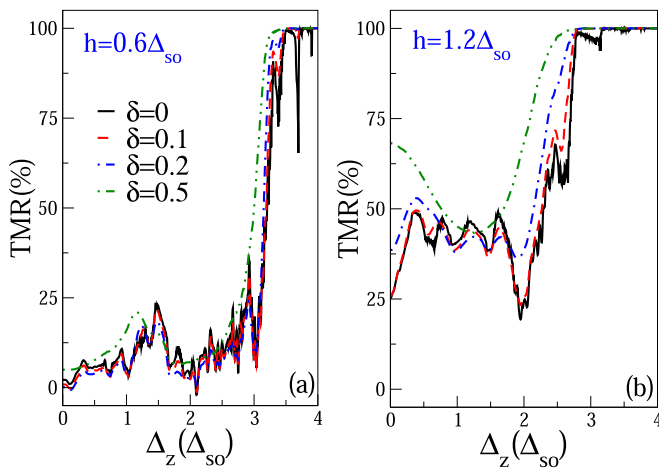
FIG. 15. TMR of D-MSSLs as a function of $\Delta_z$ at different intensities of the disorder associated to the strength of the magnetic barriers. The exchange field strengths considered are (a) $h = 0.6\Delta_{SO}$ and (b) $h = 1.2\Delta_{SO}$. The other superlattice parameters are the same as in the preceding figures.

port properties, respectively. Our results indicate that the structural disorder instead of deteriorating the magnetoresistance and the spin-valley polarization helps to improve them. The improvement relies on the elimination of the oscillations in the transport properties caused by the periodic magnetic modulation. In particular, the alternate regions of negative and positive 100% spin-valley polarization in the antiparallel magnetization configuration transform in a region of negative 100% spin-valley polarization, opening the door for two well-defined spin-valley polarization states reachable by simply switching the magnetization configuration. Regarding the tunneling magnetoresistance, the disorder flattens the regions of high TMR, resulting in a region of 100% TMR that can be enlarged by increasing the disorder intensity. These findings indicate that in designing versatile silicene superlattice devices with magnetoresistive and spin-valleytronic capabilities it is more convenient to allow moderate structural disorder instead of trying to eliminate it.

[1] C.-H. Park, L. Yang, Y.-W. Son, M. L. Cohen, and S. G. Louie, Nat. Phys. **4**, 213 (2008).

[2] M. Barbier, P. Vasilopoulos, and F. M. Peeters, Phys. Rev. B **81**, 075438 (2010).

[3] S. Dubey, V. Singh, A. K. Bhat, P. Parikh, S. Grover, R. Sensarma, V. Tripathi, K. Sengupta, and M. M. Deshmukh, Nano Lett. **13**, 3990 (2013).

[4] L. A. Ponomarenko, R. V. Gorbachev, G. L. Yu, D. C. Elias, R. Jalil, A. A. Patel, A. Mishchenko, A. S. Mayorov, C. R. Woods, J. R. Wallbank, M. Mucha-Kruczynski, B. A. Piot, M. Potemski, I. V. Grigorieva, K. S. Novoselov, F. Guinea, V. I. Fal'ko, and A. K. Geim, Nature (London) **497**, 594 (2013).

[5] C. R. Dean, L. Wang, P. Maher, C. Forsythe, F. Ghahari, Y. Gao, J. Katoch, M. Ishigami, P. Moon, M. Koshino, T. Taniguchi, K. Watanabe, K. L. Shepard, J. Hone, and P. Kim, Nature (London) **497**, 598 (2013).

[6] B. Hunt, J. D. Sanchez-Yamagishi, A. F. Young, M. Yankowitz, B. J. Leroy, K. Watanabe, T. Taniguchi, P. Moon, M. Koshino, P. Jarrillo-Herrero, and R. C. Ashoori, Science **340**, 1427 (2013).

[7] J. Barrier, P. Kumaravadivel, R. K. Kumar, L. A. Ponomarenko, N. Xin, M. Holwill, C. Mullan, M. Kim, R. V. Gorbachev, M. D. Thompson, J. R. Prance, T. Taniguchi, K. Watanabe, I. V. Grigorieva, K. S. Novoselov, A. Mishchenko, V. I. Fal'ko, A. K. Geim, and A. I. Berdyugin, Nat. Commun. **11**, 5756 (2020).

[8] R. Bistritzer and A. H. MacDonald, Proc. Natl. Acad. Sci. USA **108**, 12233 (2011).

[9] Y. Cao, V. Fatemi, S. Fang, K. Watanabe, T. Taniguchi, E. Kaxiras, and P. Jarrillo-Herrero, Nature (London) **556**, 43 (2018).

[10] P. Rickhaus, F. K. de Vries, J. Zhu, E. Portoles, G. Zheng, M. Masseroni, A. Kurzmann, T. Taniguchi, K. Watanabe,

A. H. Macdonald, T. Ihn, and K. Ensslin, Science **373**, 1257 (2021).

[11] C. Forsythe, X. Zhou, K. Watanabe, T. Taniguchi, A. Pasupathy, P. Moon, M. Koshino, P. Kim, and C. R. Dean, Nat. Nanotechnol. **13**, 566 (2018).

[12] S.-C. Chen, R. Kraft, R. Danneau, K. Richter, and M.-H. Liu, Commun. Phys. **3**, 71 (2020).

[13] S. Cahangirov, M. Topsakal, E. Aktürk, H. Şahin, and S. Ciraci, Phys. Rev. Lett. **102**, 236804 (2009).

[14] A. Kara, H. Enriquez, A. P. Seitsonen, L. C. L. Y. Voon, S. Vizzini, B. Aufray, and H. Oughaddou, Surf. Sci. Rep. **67**, 1 (2012).

[15] J. Zhao, H. Liu, Z. Yu, R. Quhe, S. Zhou, Y. Wang, C. C. Liu, H. Zhong, N. Han, J. Lu, Y. Yao, and K. Wu, Prog. Mater. Sci. **83**, 24 (2016).

[16] C.-C. Liu, W. Feng, and Y. Yao, Phys. Rev. Lett. **107**, 076802 (2011).

[17] C.-C. Liu, H. Jiang, and Y. Yao, Phys. Rev. B **84**, 195430 (2011).

[18] N. D. Drummond, V. Zólyomi, and V. I. Fal'ko, Phys. Rev. B **85**, 075423 (2012).

[19] Z. Ni, Q. Liu, K. Tang, J. Zheng, J. Zhou, R. Qin, Z. Gao, D. Yu, and J. Lu, Nano Lett. **12**, 113 (2012).

[20] Q. Zhang, K. S. Chan, and J. Li, Sci. Rep. **6**, 33701 (2016).

[21] W. Li, W.-T. Lu, Y.-F. Li, and H.-H. Han, Physica E **88**, 284 (2017).

[22] W.-T. Lu, Y.-F. Li, and H.-Y. Tian, Nanoscale Res. Lett. **13**, 84 (2018).

[23] S.-K. Wang and J. Wang, Chin. Phys. B **24**, 037202 (2015).

[24] S. Mirershadi and F. Sattari, Physica E **115**, 113696 (2020).

[25] F. Sattari and S. Mirershadi, Physica E **124**, 114287 (2020).

[26] N. Missault, P. Vasilopoulos, V. Vargiamidis, F. M. Peeters, and B. Van Duppen, Phys. Rev. B **92**, 195423 (2015).

[27] Z. P. Niu, Y. M. Zhang, and S. Dong, New J. Phys. **17**, 073026 (2015).

[28] N. Missault, P. Vasilopoulos, F. M. Peeters, and B. Van Duppen, Phys. Rev. B **93**, 125425 (2016).

[29] Z. Rashidian, Z. Lorestaniweiss, Y. Hajati, S. Rezaeipour, and G. Rashedi, J. Magn. Magn. Mater. **442**, 15 (2017).

[30] Z. Rashidian, Y. Hajati, S. Rezaeipour, and S. Baher, Physica E **86**, 111 (2017).

[31] L.-L. Chang, Q.-P. Wu, R.-L. Zhang, Y.-Z. Li, M.-R. Liu, X.-B. Xiao, and Z.-F. Liu, Phys. B: Condens. Matter **601**, 412552 (2021).

[32] J. G. Rojas-Briseño, M. A. Flores-Carranza, P. Villasana-Mercado, S. Molina-Valdovinos, and I. Rodríguez-Vargas, Phys. Rev. B **103**, 155431 (2021).

[33] F. Sattari and S. Mirershadi, Eur. Phys. J. B **91**, 259 (2018).

[34] O. Oubram, O. Navarro, E. J. Guzmán, and I. Rodríguez-Vargas, Superlattices Microstruct. **113**, 483 (2018).

[35] N. Abedpour, A. Esmailpour, R. Asgari, and M. R. R. Tabar, Phys. Rev. B **79**, 165412 (2009).

[36] A. Esmailpour, H. Meshkin, and R. Asgari, Solid State Commun. **152**, 1896 (2012).

[37] A. Esmailpour, H. Meshkin, and M. Saadat, Physica E **50**, 57 (2013).

[38] A. Esmailpour, M. Abdolmaleki, and M. Saadat, Physica E **77**, 144 (2016).

[39] O. Oubram, O. Navarro, E. J. Guzmán, and I. Rodríguez-Vargas, Physica E **120**, 114100 (2020).

[40] T. Yokoyama, Phys. Rev. B **87**, 241409(R) (2013).

[41] A. Yamakage, M. Ezawa, Y. Tanaka, and N. Nagaosa, Phys. Rev. B **88**, 085322 (2013).

[42] J. S. Moodera and G. Mathon, J. Magn. Magn. Mater. **200**, 248 (1999).

[43] R. Saxena, A. Saha, and S. Rao, Phys. Rev. B **92**, 245412 (2015).

[44] F. Banfi, V. Bellani, I. Gómez, E. Diez, and F. Domínguez-Adame, Semicond. Sci. Technol. **16**, 304 (2001).